Atmos. Chem. Phys. Discuss., 8, 16175–16218, 2008
www.atmos-chem-phys-discuss.net/8/16175/2008/

Atmospheric Chemistry and Physics Discussions

This discussion paper is/has been under review for the journal *Atmospheric Chemistry and Physics (ACP)*. Please refer to the corresponding final paper in *ACP* if available.

Seasonal variation of temperatures between 1 and 105 km altitude at 54° N observed by lidar

M. Gerding, J. Höffner, J. Lautenbach, M. Rauthe, and F.-J. Lübken

Leibniz-Institute of Atmospheric Physics, Kühlungsborn, Germany

Received: 2 July 2008 – Accepted: 29 July 2008 – Published: 26 August 2008

Correspondence to: M. Gerding (gerding@iap-kborn.de)

Published by Copernicus Publications on behalf of the European Geosciences Union.

Abstract

Temperature soundings are performed by lidar at the mid-latitude station of Kühlungsborn (Germany, 54° N, 12° E). The profiles cover the complete range from the lower troposphere (~1 km) to the lower thermosphere (~105 km) by simultaneous and co-located operation of a Rayleigh-Mie-Raman lidar and a potassium resonance lidar. Observations have been done during 266 nights between June 2002 and July 2007, each of 3–15 h length. This large and unique data set provides comprehensive information on the altitudinal and seasonal variation of temperatures from the troposphere to the lower thermosphere. The remaining day-to-day-variability is strongly reduced by harmonic fits at constant altitude levels and a representative data set is achieved. This data set reveals a two-level mesopause structure with an altitude of about 86–87 km (~144 K) in summer and ~102 km (~170 K) during the rest of the year. The average stratopause altitude is ~48 km throughout the whole year, with temperatures varying between 258 and 276 K. From the fit parameters amplitudes and phases of annual, semi-annual, and quarter-annual variations are derived. The amplitude of the annual component is largest with amplitudes of up to 30 K in 85 km, while the quarter-annual variation is smallest and less than 3 K at all altitudes. The lidar data set is compared with ECMWF temperatures below about 70 km altitude and reference data from the NRLMSISE-00 model above. Apart from the temperature soundings the aerosol backscatter ratio is measured between 20 and 35 km. The seasonal variation of these values is presented here for the first time.

1 Introduction

Temperature is one of the most fundamental and important quantities to describe the Earth's atmosphere. The altitudinal and seasonal variations are a result of radiative, chemical, and dynamical effects (cf., e.g., Garcia, 1989). Radiative forcing has the main effect on the background temperature structure, e.g. the middle atmosphere is

ACPD

8, 16175–16218, 2008

heated by the absorption of solar UV radiation by O_2 and O_3 (Mlynczak and Solomon, 1993) and cooled by the emission of infrared radiation by CO_2 (Andrews et al., 1987). Dynamical forcing produces major deviations from the radiative equilibrium in the middle atmosphere. Direct energy deposition by wave dissipation is added by momentum deposition, slowing down or reversing the zonal wind. This results in a strong meridional circulation, which is connected with upwelling (summer) and downwelling (winter) above the poles and mid-latitudes, i.e. with adiabatic cooling and heating (Lindzen, 1981; Holton, 1982). Exothermic chemical reactions provide an additional heat source of the atmosphere, while airglow in the mesopause region or chemiluminescence are acting as energy sinks (Riese et al., 1994).

Detailed and high-resolved observations of the temperature structure are strongly needed for the examination of the atmosphere's energy budget, dynamics and chemistry. Temperature data sets can be used for the validation of General Circulation Models (GCM) etc. State-of-the-art GCMs often cover the whole range from the troposphere to the (lower) thermosphere, reflecting the importance of vertical coupling for the description of the atmospheric state. In contrast to this many observational techniques can only be used in a limited altitude range. Comparisons therefore require the combination of different techniques with their individual limitations. E.g. radiosondes provide a high altitude resolution (~100 m) in the troposphere and lower stratosphere, but are often limited to one or two profiles per day and altitudes below ~30 km. Disturbing effects of natural variability can often be reduced by multi-year averaging. Satellite soundings become increasingly important as they cover partly extended altitudes from the stratosphere to the lower thermosphere (e.g. Shepherd et al., 2001; Mertens, 2001; Xu et al., 2007). They provide a global view, but due to orbit constraints they need long data series to overcome drawbacks of zonal averaging and/or local time coverage. The vertical resolution is often in the range of 3–4 km, i.e. worse than many GCMs. Systematic errors might occur due to non-local thermodynamic equilibrium especially in the summer mesopause region at mid and high latitudes (Kutepov et al., 2006) or difficulties in the calculation of geometric altitudes (Sica et al., 2008). GPS radio occultations

ACPD
8, 16175–16218, 2008

provide a good local time and zonal coverage, but are limited to the troposphere and (low/mid) stratosphere (e.g. Gobiet et al., 2005). Various types of rocket soundings have been performed to measure temperatures in the mesosphere at several locations (e.g. Lübken, 1999; Lübken et al., 2004). The lack of temporal resolution can be avoided by combination of different data sets at a single locations. Unfortunately, rocket soundings are still sparse, especially at mid-latitudes, and provide typically only snapshots of the atmosphere (e.g. Hirota, 1984; Kubicki et al., 2006). Lidar observations are as well limited to a few fixed locations. Depending on the particular technique typical altitude ranges are 0–30 km, 30–80 km, or 80–110 km (cf., e.g. Hauchecorne et al., 1991; Yu and She, 1995; Wickwar et al., 1997; Leblanc et al., 1998; States and Gardner, 2000; Friedman and Chu, 2007). Time resolved observations allow the identification of gravity waves and tides that average out in the nightly or daily mean. Typical altitude resolutions of ∼1 km are fine compared to satellite data.

In this paper we describe the temperature structure at Kühlungsborn (Germany, 54° N, 12° E). Although that this is a mid-latitude site, it is still influenced by polar phenomena like Noctilucent Clouds (NLC) (cf. Gerding et al., 2007b) or Sudden Stratospheric Warmings (SSW). This makes an important difference to more equatorward stations like Observatoire d'Haute Provence, France at 44° N (Hauchecorne et al., 1991), Fort Collins, Colorado at 41° N (Yu and She, 1995) or Urbana, Illinois at 40° N (States and Gardner, 2000), even if they are only separated by a few degrees in latitude. The temperature structure at the latitude of 54° N provides an important benchmark for general circulation models as well as substantial information for retrieval of atmospheric parameters from satellite soundings. As our site is located at the edge of the Noctilucent Cloud/Polar Mesospheric Cloud (NLC/PMC) existence region, it provides a reference point for the understanding of ice particle generation and potential NLC/PMC trends. The seasonal variation of gravity wave activity has recently been published by Rauthe et al. (2008) for part of the data described here.

We present a summary of more than 1850 h of data. By use of three different scattering types and combination of two lidars an altitude range between 1 and 105 km is

covered with identical temporal and spatial resolution. To the best of our knowledge this is the first comprehensive temperature data set covering the whole range from the troposphere to the lower thermosphere. In the following we first give an update on our lidar systems. In Sect. 3 we present the temperature observations for the period June 2002 to July 2007. A harmonic fit of the temperature variation is calculated for each single altitude bin. By this the natural variability is blanked and a more representative data set is obtained (Sect. 4). Of particular interest are the temperatures and altitudes of the mesopause and stratopause that are presented in Sect. 5. In Sect. 6 we compare our data with the most recent MSIS climatology (NRLMSISE-00, cf. Picone et al., 2002) and ECMWF analyses. In the last section we discuss our results and compare with other ground-based and space-based observations.

2 Description of the lidar systems

At the Leibniz-Institute of Atmospheric Physics we combine a Rayleigh-Mie-Raman (RMR) lidar (Alpers et al., 2004) and a potassium resonance lidar (K lidar) (von Zahn and Höffner, 1996) to achieve temperature profiles from the troposphere to the lower thermosphere. The RMR lidar uses the well known Rayleigh temperature retrieval (hydrostatic integration of the density profile) and the rotational Raman method. Our lidar systems and the combination of the methods are described by Alpers et al. (2004). Below we show an example of a temperature sounding from June 2005 and describe recent updates of the setup.

The temperature profiles at Kühlungsborn are a combination of potassium resonance temperatures (~85–105 km), Rayleigh temperature profiles in two altitude ranges using separate telescopes and detectors (~44–85 km and 34–46 km), aerosol-corrected Rayleigh-temperature profiles (~22–33 km), and rotational Raman temperatures (~1–25 km). Figure 1 (left) shows an example of a temperature profile at 20 June 2005 with 1 km vertical resolution after 1 h of integration (22:30–23:30 UT). The individual methods are displayed in different colors. The potassium lidar covers the range from the

ACPD
8, 16175–16218, 2008

top of the profile down to 85 km altitude due to the limited extension of the K layer in summer (cf. Eska et al., 1998). The Mesosphere-Rayleigh channel provides temperatures below 86 km using the K lidar observations at 88 km as a start value for density integration. This channel measures down to 44 km altitude. The data at 48 km are used as a start value for the Stratosphere-Rayleigh channel yielding data between 46 and 22 km altitude. Below 34 km this channel is corrected for additional aerosol backscatter (see below). The rotational Raman temperatures are used below 25 km. The error bars at the particular profiles denote the uncertainty of photon count statistics. The typical statistical uncertainty is about 2–3 K. In this study we only use data points with an uncertainty of less than 10 K. We will concentrate on nightly averages calculated from hourly profiles like the example in Fig. 1. The statistical uncertainty of nightly means is strongly reduced compared to the single profiles and depends on the length of the sounding. In the following we will partly neglect the statistical uncertainty since it is small compared to the natural variability (typically 4–10 K depending on altitude and season). The right part of Fig. 1 shows in detail the profiles in the troposphere and lower stratosphere. A simultaneous temperature profile from a co-located radiosonde launch is presented for comparison (red line). The lidar integration time covers approximately the flight time from the ground to the tropopause, whereas the stratospheric part of the radiosonde profile is observed after the lidar integration time. The tropospheric temperatures agree nearly perfectly except for the lowest data point of the lidar profile. The gradients in the tropopause region are partly underestimated by the lidar due to its coarser altitude resolution. In the stratosphere the in-situ and remote-sensed data agree well, taking the increasing horizontal and temporal distance between lidar and drifting radiosonde into account (max ∼30 km, 1 h).

Hydrostatic temperature retrievals from elastic backscatter are affected by the presence of aerosols, as the backscatter is no longer proportional to the density. The mesosphere and upper stratosphere are normally anticipated as aerosol-free. However, in the lower stratosphere there is a background aerosol layer that might extend well above 20 km. To correct for any additional aerosol backscatter at the 532 nm wave-

ACPD
8, 16175–16218, 2008

length channel used for the Rayleigh temperature retrieval, we have simultaneously observed the 608 nm N_2 vibrational Raman backscatter (Gerding et al., 2006). This is used to calculate the backscatter ratio R of total and molecular backscatter on a nightly mean basis. We have corrected every elastic backscatter profile applying R to yield the true density profile needed for the temperature retrieval. Figure 1 shows the Rayleigh temperatures with and without aerosol correction as solid and dotted green lines, respectively. After the correction the lidar observed temperature profile shows perfect agreement with the radiosonde observation. The aerosol-induced bias is largest in the lowest Rayleigh channels (up to ~7 K) and remains visible up to about 31 km. The aerosol correction based on observed R profiles is available since February 2004. Before that date, an aerosol correction based on an empirical average R profile has been applied (Alpers et al., 2004).

The N_2 vibrational Raman backscatter is observed up to ~50 km altitude. It is taken as a measure for the molecular backscatter after normalization to the 532 nm signal at an aerosol-free altitude. The latter contains both molecular and aerosol backscatter (i.e. total backscatter). The normalization is taken at about 34 km altitude to avoid errors due to the decreasing photon statistics above. The atmosphere is assumed to be aerosol free above this altitude, in good agreement with other observations (e.g. Vaughan and Wareing, 2004). The aerosol correction provides a data set of backscatter ratios in a height region that is rarely covered by regular aerosol soundings from lidars and satellites. By our regular N_2 Raman soundings we yielded for the first time an extensive ensemble of backscatter ratios in the mid-stratosphere. The data sets covers 213 lidar observations since 11 February 2004, each of more than 3 h duration.

Figure 2 shows the seasonal variation of the backscatter ratio R in the altitude range 20–35 km. Between March and October only small seasonal variations of R occur. After smoothing across ±30 days some variability remains. But this is mostly due to a high night-to-night variability (not shown here) and less induced by periodic seasonal variations. Between December and February and in August/September an increase in the backscatter ratio in the 20–30 km range is obvious. Above 30 km, again any

potential seasonal variation remains hidden behind variability on the scale of days. Independent from season the backscatter ratio decreases with altitude up to the upper end of our observation range (here: 34 km, with R=1.0 by definition). As a rule of thump we observe a backscatter ratio R=1.1 at 21 km, R=1.06 at 23–24 km, R=1.04 at 25 km, and R=1.02 around 28 km. Above 30 km we mostly observed R<1.01.

3 Seasonal variation of temperatures from observed data

The lidar observations at Kühlungsborn were performed throughout the five years whenever weather conditions allowed. 266 nights of lidar operation between June 2002 and July 2007 are used for this study, each of at least 3 h and up to 15 h combined operation of K lidar and RMR lidar. With this data set all seasons are covered, but with less soundings in winter due to bad weather conditions. Figure 3 gives an overview on the distribution of nights throughout the seasons. Each nightly mean profile shows the temperature in color coding. The figure provides also a histogram with the number of observations per night (e.g. 1 at 7, 9 and 10 January, and 2 at 15 January, ...). Only few periods of about two weeks without sounding can be found in Fig. 3. Nevertheless, several dates have been sampled more than once within the five years. Almost all profiles reach an altitude of 100 km, and most of the data extend up to 105 km and above. Only in summer some gaps between 100 and 105 km exist due to the limited extension of the K layer (Eska et al., 1998). Above 105 km the number of data points decreases and the seasonal coverage gets worse. Therefore we limit all further studies of the mean state and seasonal variations to the height range of 1–105 km.

Some general features of the temperature structure above Kühlungsborn can be identified from Fig. 3.

i) Most obvious is the cold summer mesopause between 85 and 90 km.

ii) Part of the winter data show a comparatively warm stratopause.

iii) During winter the night-to-night variability in stratopause region and mesosphere is high.

We will address these topics in more detail later. To reduce the night-to-night variability we have calculated monthly mean profiles, averaging e.g. all January nightly mean observations of the different years to a single profile. Figure 4 and Table 1 show the monthly mean profiles and their standard deviations (based on nightly averages). First we concentrate on absolute temperatures. In the lower stratosphere between about 10 and 30 km two seasons can be distinguished: The winter season covers the months November to February and is characterized by a temperature decrease with altitude. During the rest of the year there is partly a small range with nearly constant temperatures up to about 25 km, but a general positive gradient between tropopause and 30 km altitude. In several months (independent from season) a small temperature inversion is visible above the tropopause. The stratopause in the monthly means is always slightly below 50 km, with the exception of January (43 km) and November (52 km). For the mesopause altitude the monthly means reveal two states: Between May and August the temperature has a pronounced minimum at 86/87 km. The mesopause temperature drops down to ~144 K in June/July. Compared to this, May and August are about 10 and 15 K warmer. During the rest of the year the mesopause altitude is slightly above 100 km, and by this partly not covered by the monthly means. We point out here that the transition between both periods is very fast (see below), i.e. a mixed state does not exist in terms of monthly means and a double mesopause (cf., e.g. She et al., 1993; Berger and von Zahn, 1999) is not observed. Mesopause observations within individual nights are described later.

The standard deviations of the nightly means also have a distinct altitudinal and seasonal variation (Fig. 4). The variability is generally larger in winter and smaller in summer. The strongest seasonal effect occurs in the upper stratosphere and lower mesosphere where the standard deviation varies by a factor of ~4–10 (cf. Rauthe et al., 2008). The high variability in winter is mostly due to planetary wave activity and interannual variability. The altitudinal variation also depends on season. Between January

ACPD
8, 16175–16218, 2008

and May the standard deviation initially decreases with altitude around the stratopause and increases again above ∼60 km. Between October and December only a small range of reduced variability in the mesosphere can be found. Additionally, there is an obvious decrease in the standard deviation in the upper mesosphere in November and December. The high variability in the range between 70 and 80 km, is due to so-called mesospheric inversion layers (MIL) (see, e.g. review by Meriwether and Gerrard, 2004) and strong gravity and tidal waves, remaining in the nightly mean profiles even after integration of up to ∼15 h. Further analysis of gravity wave signatures in our lidar observed temperatures is presented by Rauthe et al. (2006, 2008). The analysis of MIL is outside the scope of this paper.

4 Harmonic fit of temperatures

The night-to-night variability implies some difficulties to extract an undisturbed representative temperature structure for our location even with our extended data base. We compare the seasonal dependent night-to-night and interannual variability for different altitudes (30, 65, 74, 87 km) in Fig. 5. The individual nightly mean temperatures are given as single dots. Additionally, the figure shows smoothed and fitted data of the temperature. We have chosen a Hanning filter with ±30 d width to eliminate all variations with scales shorter than about one month. A representative mean temperature is calculated by harmonic fits. Harmonic fits inherently provide some periodic seasonal variation. The harmonic fit presented here uses at first an annual variation due to the changing illumination from the sun. A semi-annual harmonic is added due to some dynamic processes like the observed stratospheric warmings that are of different phase as the solar irradiance. A quarter annual component has been added to identify the characteristics of the remaining variations. It will be shown later that this harmonic is only of minor importance. In summary we use a harmonic equation of the form

$$T(z,t)=A_0+A_1\cdot\cos(\omega_1\cdot(t-\varphi_1))+A_2\cdot\cos(\omega_2\cdot(t-\varphi_2))+A_3\cdot\cos(\omega_3\cdot(t-\varphi_3)) \quad (1)$$

ACPD
8, 16175–16218, 2008

with $A_0(z)$ mean temperature at altitude z, t time in days, $A_i(z)$ and $\varphi_i(z)$ amplitudes and phases of the annual ($i=1$), semi-annual ($i=2$) and quarter-annual ($i=3$) variations. $\omega_i = \frac{2\pi}{P_i}$ describes the frequency, with P_i the period (in days) of the different variations.

At 30 km the night-to-night variability of temperatures is generally small (standard deviation ~3–5 K, cf. Fig. 4). Only during the winter season (October–March) the temperature deviates by up to 25 K from the mean due to planetary wave activity. The temperatures vary strongly with season with a peak-to-peak value of ~25 K. In the lower mesosphere at 65 km the seasonal variation is strongly reduced compared to 30 km, i.e. it is smallest compared to all altitudes below 100 km. By this, the seasonal variation is partly lower than the night-to-night variation at this altitude. The latter is strongest in winter, related to mesospheric cooling events accompanying stratospheric warmings. The average temperature at 65 km decreases continuously in time by about 10 K between June and September, followed by a fast increase of 10 K till the end of October. The Hanning filtered data sets shows some strong variation between October and January, but this data set obviously does not represent a mean state but is affected by the high variability and a bad sampling due to weather conditions. The harmonic fit eliminates this signatures of the smoothed time series, while the observed nightly averages are still nicely reproduced. In other words, the fitted time series can be anticipated as the best representation of the data and as a mean state in a climatological sense.

At 74 km a distinct seasonal variation is again obvious. The peak-to-peak value is about 30 K with the minimum in summer as expected for the upper mesosphere. The night-to-night variability is generally higher than below, but still about four times higher in winter than in summer. Again, the smoothed time series shows some variations that are partly due to a bad sampling in winter, while the harmonic fit nicely represents the winter data. The largest seasonal variation is observed in the region around 87 km altitude. In average it is up to about 50 K, with the difference between extreme values being much higher (nearly 100 K). In April and May the temperatures decrease fast and are minimal in the high summer at June/July. Conversely, in August a fast increase of

ACPD
8, 16175–16218, 2008

temperatures at 87 km is observed. The cold summer season is much shorter than the winter. In winter the night-to-night-variability at 87 km is about as large as in the mid-mesosphere, whereas the summer variability is increased compared to lower altitudes. The harmonic fit reproduces not only the general behavior of temperatures at 87 km altitude, but also the fast transitions in April and August as well as the temperature minimum in June/July. The temperature minimum of ∼144 K occurs nearly at summer solstice around day 169 (18 June).

The fitted data allow to determine the slopes of the temperature changes within a particular altitude. The seasonal variation is more or less asymmetric at all altitudes displayed in Fig. 5. At 30 and 74 km the temperature change in spring is slower than the autumn change (about 0.15 K/d and −0.2 K/d in spring, −0.2 K/d and 0.25 K/d in autumn, respectively). At 87 km spring and autumn slope are similar (∓0.5 K/d). This slope results in a temperature decrease (increase) by ∼20 K within a single month. The fast temperature change leads to the quasi non-existence of a double mesopause in spring/autumn at our site.

At 65 km the slope is different due to the low seasonal variation. Here the average temperature decrease between mid of May and mid of September is −0.1 K/d, followed by an increase until November. The change of the slope in September/October is too fast to be captured by the harmonic analysis. For the other seasons the fit reveals nearly constant temperatures at 65 km. We will examine amplitudes and phases of the different harmonics later in more detail.

Figure 6 shows a) the fitted climatological mean temperature structure for the whole range between 1 and 105 km at Kühlungsborn and b) the difference between the observed and fitted temperature structure. The data of Fig. 6a are tabulated in the supplement http://www.atmos-chem-phys-discuss.net/8/16175/2008/acpd-8-16175-2008-supplement.pdf of this publication for intervals of 10 d and 3 km, the altitude-dependent fit parameters are described below. The fit results from annual, semi-annual and quarter-annual harmonic fits as described above. The dipole structure in summer with a warm summer stratopause and a cold mesopause is clearly visible.

ACPD
8, 16175–16218, 2008

The temperature in the stratosphere has a clear annual variation with a minimum in winter. Above the stratopause the amplitude of the seasonal variation decreases and the phase reverses, producing a nearly isothermal layer around 65 km. In the upper mesosphere the isolines of temperatures clearly show the asymmetry in the seasonal variation with a faster autumn transition. A downward progression of the cold phase is indicated between 55 and 105 km. The promincence of the warm winter stratopause is strongly reduced compared to the single observations displayed in Fig. 3 (265 K to about 300 K in single nights), but the temperature increase from autumn to winter is still clearly visible. In Sect. 5 we will examine the altitudes and temperatures of the stratopause and mesopause as the most remarkable features of the temperature structure above Kühlungsborn. Figure 6b shows the difference between the observed nightly mean profiles (cf. Fig. 3) and the harmonic fit. The differences are smoothed in time by a ±10 day Hanning filter to yield a better visualization of the differences. In general the harmonic fit nicely represents the general features of the observed temperature structure. There are neither altitude ranges nor seasons with a bias between the pure observations and the fit. For most of the seasons the difference is less than 5 K at all altitudes. Only in winter larger differences occur. As the differences are both negative and positive they are mostly due to natural night-to-night and year-to-year variability, i.e. planetary wave activity. In December and January a slight cold-bias of the fitted temperatures in the stratopause region and a warm-bias in the mesosphere exist, indicating that the highly variable temperature structure in the stratopause region can not be described in full detail with our harmonic analysis.

Amplitudes and phases of the annual, semi-annual, and quarter-annual components vary strongly with altitude (Fig. 7 and Table 2). The annual component dominates nearly at all altitudes. It is largest at 85 km altitude with an amplitude of nearly 28 K (i.e. peak-to-peak value of 56 K). Other maxima are found in the lowermost mesosphere, the mid-stratosphere and the troposphere. The semi-annual component is strongest around 43 km and 87 km. The quarter-annual component is always small and its amplitude does not exceed 3 K. Therefore, generally annual and semi-annual variations

ACPD
8, 16175–16218, 2008

are sufficient to describe the seasonal variation at all altitudes.

In Fig. 7b we have plotted the phase maxima (i.e. the days where the temperature is maximal) for every altitude where the amplitude of the fit exceeds 1 K. In the other regions the phases can not be estimated exactly and the particular harmonic component is of only minor importance. The annual component in the upper mesosphere has a phase maximum in winter due to the higher winter temperatures. Around 65 km there is a fast phase shift by about 4 months due to the summer dipole character of the stratopause and mesopause. Below 55 km the annual component is always in the summer phase with only slight shifts in the order of one month. At the tropopause a distinct phase jump of one month is observed, resulting in a phase maximum near the end of July. The tropospheric and stratospheric phases can be explained by the influence of the sun. The tropospheric weather reacts with a delay of about one month to the changing solar elevation. The stratosphere is more radiatively controlled especially by the absorption of light by ozone. The phase of temperature changes synchronously to the sun. The winter phase maximum in the upper mesosphere is independent from the solar irradiation. It is well known that the mean temperatures in the upper mesosphere are more dynamically than radiatively controlled.

The phase maxima of the semi-annual component are e.g. at the end of March around 85 km and at the end of June around 45 km. In the stratopause region the phase is clearly due to the two maxima in stratopause temperatures in summer and winter. In the region between 80 and 90 km there is no direct geophysical reason for the phase maximum. Here the phasing produces the fast temperature change in spring and autumn. The quarter-annual component is always small, as described above. However, its phase is strongly coupled to the phase of the semi-annual fit. This gives reason for the assumption that the quarter-annual variation has no own geophysical cause but occurs as a higher harmonic.

A remarkable similarity also exists in the phase velocities of the different harmonics. Nearly always negative phase velocities are observed, indicating a top-down propagation of temperature phenomena. The phase velocities of the semi- and quarter-annual

ACPD
8, 16175–16218, 2008

component are about −0.4 km/d in the whole range between 45 and 90 km. The same is true for the annual component between 70 and 90 km.

5 Seasonal variation of stratopause and mesopause

The continuous set of temperature profiles between 1 and 105 km allows to observe the stratopause and mesopause by the same instrumental technique. Even though our observations cover also the tropopause region, we have to acknowledge that other data sets like radiosonde climatologies provide a much better resolution at this heights. Therefore we concentrate on the stratopause and mesopause, with their temperatures and altitudes shown in Fig. 8. The temperature extrema calculated from the nightly mean profiles are plotted as single data points in black. Nightly means are still affected by different kinds of waves (gravity, tidal, planetary) which reduces e.g. the comparability with other data sets and models. Therefore we also plotted the fitted temperature field (red line) and interpret only these as stratopause and mesopause. It should be noted that especially the mesopause can not always be identified from our data set (individual points and fit), as temperatures in winter partly decrease up to the top of the profiles.

The altitude of the stratopause is nearly constant throughout the year. It varies between 47 and 49 km without any clear seasonal cycle. The altitude of the temperature maximum in individual nights might differ by up to ∼10 km from the "climatological" stratopause. In contrast to the altitude of the stratopause its temperature has a clear semiannual cycle with a winter maximum due to the stratospheric disturbances already mentioned above. The summer stratopause (∼275 K) is slightly warmer than the winter stratopause (∼266 K). Also the spring/autumn minima in stratopause temperatures are not identical, but autumn temperatures more than 5 K lower. Looking at the seasonal variation of stratopause temperatures maxima occur around solstices, while minima are before (spring) and after (autumn) equinoxes.

Mesopause altitudes vary by about 15 km throughout the year. This variation is by

ACPD
8, 16175–16218, 2008

far not harmonic but can be represented with a bi-stable state with the mesopause being in the lower level for about 120 days between May and August and in the higher level (∼102 km) for the rest of the year. Within the summer months a slight altitude decrease from 87 to 85 km is observed, following the temperature decrease (shrinking) in the upper mesosphere during summer. The transition between the upper and lower mesopause level is nearly instantaneous and an intermediate state practically non-existing. Only within single nights the temperature minimum is found between 90 and 95 km. But here effects of gravity and tidal waves have to be taken into account, which might remain in the data even after some hours of observations. The temperature of the mesopause changes more continuously, especially in summer when the mesopause is low. The temperature minimum of ∼144 K occurs around day 169, i.e. a few days before summer solstice. The transition to the upper-level-period of the mesopause is smooth and the temperatures during that time more variable. Between September and April the mesopause temperature shows no distinct seasonal variation but is in average roughly constant at ∼170 K with high night-to-night variability. Overall, the temperature of the mesopause changes throughout the year by ∼30 K, i.e. much less than the temperature variation at about 87 km.

6 Comparison with climatologies and analyses

The temperature profiles observed above Kühlungsborn by lidar are compared with other data both on a climatological and an event basis. In the following we compare our data with the most recent reference atmosphere NRLMSISE-00 (Picone et al., 2002) above ∼65 km and the meteorological analyses from the European Center for Medium Range Weather Forecast (ECMWF) below. The ECMWF model assimilates various observations from satellites, balloons and groundbased stations. By this they provide the most representative data set for the troposphere and stratosphere. Above that region observations and model results have been summarized in the NRLMSISE-00 climatology. Recently we have compared our data also with temperature data of the

ACPD
8, 16175–16218, 2008

FTS instrument onboard the ACE-SCISAT satellite and found differences especially in the summer mesopause region (Sica et al., 2008). In this region a known bias exists in many satellite measurements of temperature (cf. Kutepov et al., 2006). For further comparisons we refer to the discussion section of this paper.

In Fig. 9 the differences of the lidar temperature profiles and the combined NRLMSISE-00/ECMWF data set are plotted. For the lidar data the result of the harmonic fit (see Fig. 6) is taken as reference. ECMWF analyses are available for every single day and 00:00, 06:00, 12:00, and 18:00 UT. We have selected the 00:00 UT profiles for all nights to get the most unbiased comparison. From NRLMSISE-00 the climatological data set for our location is used. The NRLMSISE-00 temperatures are mostly higher than the lidar observations by up to ~25 K (typically 10 K). Only for a short period after summer solstice the reference atmosphere shows lower temperatures than the mesopause region in our observations. In summary, the temperatures around 87 km are too high in the reference data set and the phase of the seasonal variation is shifted by a couple of days. In the stratopause region the high temperature difference in winter is most obvious. Especially in the beginning and end of winter the lidar observed temperatures are higher than the analyses of ECMWF. This is partly due to some suppression of stratospheric warming events in the analyses data set. Additionally, the number of lidar observations has to be increased in future winters. In the other periods and height ranges no obvious bias exists and the differences are mostly around 5 K or less.

7 Discussion

In this section we first provide a general discussion about our methods. In the second part we compare our results with other observations based on lidar and satellite soundings.

7.1 General discussion

The temperature data set presented here contains 266 observations (more than 1850 h), covering all seasons of the year with reasonable resolution. Each observation is longer than 3 h, and only profiles extending from the troposphere to the lower thermosphere are taken into account. We have shown recently by comparison with Noctilucent Clouds around 83 km that our temperature profiles are free from significant systematic errors at least in the upper mesosphere and mesopause region (Gerding et al., 2007b). The profiles are also corrected for the effect of aerosols which would induce an increasing bias below about 30 km (Gross et al., 1997; Faduilhe et al., 2005). By the averaging procedure gravity waves of 3 h, partly up to about 12 h period are smoothed out. The harmonic fit additionally removes effects of planetary waves, especially arising in the winter season.

Our observations support the concept of the two level mesopause with a lower altitude in summer and a higher level during the rest of the year (e.g. She and von Zahn, 1998). As a minor difference the start of the summer period in our observations (2002–2007) is about two weeks later than in the earlier soundings (1996–1997) presented by She and von Zahn (1998). We will come back to this topic in Sect. 6. A double mesopause structure with an inversion layer in between has been reported by States and Gardner (2000) for nighttime monthly means at 40° N based on 2 years of lidar soundings. Our data sets reveals no indications for a double mesopause even in spring and autumn as the temperature change around 87 km altitude is fast enough to establish or abolish the lower mesopause state within a few weeks.

The most important drawback of the data set presented here is the limited diurnal coverage. Some effects of diurnal tides on the true daily mean may remain, as the data presented here are obtained only during the night. States and Gardner (2000) describe some major differences in the temperature structure during day and night as measured by their lidar between 80 and 105 km at 40° N. In general the profiles covering the whole day are warmer than the nightly means below ~91 km and colder

ACPD
8, 16175–16218, 2008

between 91–100 km (by ∼5 K and ∼3 K, respectively). By this the whole temperature structure in the mesopause region is changed, and the season with a low mesopause level is shortened. A recent study of Yuan et al. (2008) for the month of April revealed higher temperatures during the night above 88 km, and slightly lower temperatures (less than 4 K compared to full-diurnal data) between 84 and 88 km. The K lidar at our station was also run during day and night for at least part of the period described here (cf. Fricke-Begemann and Höffner, 2005). We have evaluated the daily (24 h) means and the nightly means separately. E.g. for the month of June we found slightly lower temperatures in 24 h compared to nighttime-only in the whole range between 85 and 95 km, e.g. by ∼1 K in the 90 km region (not shown here). This average temperature profile might still be biased towards the nighttime-mean as only about 1/3 of all sounding hours are obtained during daylight. For the region below 85 km the RMR lidar at our site has a too bad signal-to-noise ratio during daylight to get continuous temperature profiles. In order to present a data set with the same time base for the whole altitude range we have limited this study to the nighttime soundings. The bias induced by this method is small, as the tidal effect at 54° N is small compared to the latitude of 40/41° N where the observations of States and Gardner (2000) and Yuan et al. (2008) are performed (e.g. Hagan and Forbes, 2002; Huang et al., 2006).

7.2 Comparison with other observations

There are only very few comparable data sets of aerosol backscatter ratios or similar quantities above 20 km. Fromm et al. (2003) compiled a data base of SAM II, SAGE II, and POAM II/III aerosol profiles. For our latitude they found no distinct seasonal variation but typically lower aerosol load inside the vortex than outside. Also our data with increasing backscatter ratios during the central winter period suggest some causal connection with the position of the vortex. Unfortunately, the data base of Fromm et al. (2003) shows no results above 30 km and even above 25 km the observational error becomes increasingly important. Other lidar soundings from mid-latitudes confirm our results on higher backscatter ratios in winter, even if the absolute numbers are slightly

smaller than ours (Vaughan and Wareing, 2004). The aerosol soundings demonstrate the necessity of correction methods for Rayleigh temperature retrievals in the 30 km range and below. Otherwise the atmospheric temperature may be underestimated.

Comparisons of our temperature observations with other experimental data sets are limited to partial height ranges, as other soundings typically do not cover the whole range from the troposphere to the lower thermosphere. Temperature soundings in the mesopause region are performed at our site since July 1996. Results of the first year of observations are presented by She and von Zahn (1998). The authors describe a seasonal temperature variation generally similar to our results. Nevertheless there are differences in the mesopause temperature and the amplitudes and phases of the particular harmonic components. The summer mesopause temperatures decrease by about 10 K between 1996/1997 and 2002–2007 (this data set), whereas the mesopause altitude remains unchanged. The reason for this temperature decrease remains open, as we can not distinguish from our data set between a general trend, a solar-cycle dependency or larger-scale variability. The increase of the amplitude of the annual variation in the 95 km-region (3 K to 10 K for 1996/1997 and 2002–2007) might also be due to a long-term variation, as there is some tendency for increasing amplitudes in this range if we form subsets of our database (not shown here). Minor differences occur in the phases of the harmonic fit and the summer mesopause altitude. These can be explained by the different lengths of the data sets. We note here again that She and von Zahn (1998) describe only one complete annual cycle (88 observations between July 1996 and August 1997) while our soundings cover about 5 years (266 soundings, June 2002–July 2007).

Xu et al. (2007) examined the global mesopause structure with temperature profiles from the SABER instrument onboard the TIMED satellite for the period February 2002 to February 2006. They found the nighttime summer mesopause at the latitude of Kühlungsborn around 83 km at temperatures of 145–150 K, i.e. 3–4 km lower than the mesopause in our observations, but at nearly the same temperature. Both data sets show a decrease of mesopause altitude during the summer. During the other seasons

ACPD
8, 16175–16218, 2008

the SABER mesopause is around 100 km at temperatures of ∼180 K. Again, our observations show a higher mesopause. But the mesopause temperature observed by the lidar is about 10 K lower. Both data sets agree in the slower transition between summer and normal state in spring compared to autumn.

The SABER mesopause altitudes are in agreement with the model results of the TIME-GCM (Xu et al., 2007). But the summer mesopause temperatures in the model are as low as ∼130 K which is about 15 K below both our lidar and SABER observations. Such low temperatures and the low mesopause altitude would strongly affect phenomena like Polar Mesospheric Summer Echoes and Noctilucent Clouds. However, from our simultaneous lidar soundings we found generally good agreement between temperatures and NLC. NLC appeared at the lower edge of the supersaturated altitude range and no NLC has been observed during too warm periods (Gerding et al., 2007b,a). The deficiencies of the TIMED/SABER temperature data in the polar and mid-latitude summer mesopause region are at least partly due to the non-LTE retrieval as revealed by Kutepov et al. (2006).

Huang et al. (2006) examined the signatures of the Quasi-Biennial-Oscillation (QBO) and the Semi-Annual Oscillation (SAO) in the TIMED/SABER data between 48° S and 48° N. The amplitudes and phases of the SAO in the mesosphere near 48° N are similar to the results presented here. The smaller SAO amplitudes near 85 km and near 45 km are most probably due to the latitudinal differences. In other words, the occurrence of stratospheric warmings should decrease with decreasing latitude. We note also that our study of seasonal variations show a dominating annual oscillation at nearly all altitudes.

The dominance of the annual variation is confirmed by the studies of Leblanc et al. (1998) for nighttime soundings in the range 30–105 km and Chen et al. (2000) for day and night soundings between 80 and 105 km. The latter presented differences of amplitudes of annual and semiannual variations using diurnal means or nightly means that are typically less than 25%. In general the amplitudes at Ft. Collins (41° N) are slightly smaller than at our location for both the annual and semi-annual variation (Chen et al.,

ACPD
8, 16175–16218, 2008

2000). Similar numbers are taken from the combined soundings at Ft. Collins and Observatoire de Haute Provence (44° N), covering the range 30–105 km (Leblanc et al., 1998). Here an additional maximum in the semi-annual component around 60 km has been found, which is not visible in our data at 54° N and also not in the SABER data presented by Huang et al. (2006) for 44° N. Both studies show similar phases of the annual component compared to our observation. The phase of the semi-annual variation at 41/44° N is shifted by a couple of days towards earlier times. The study of Leblanc et al. (1998) shows additionally remarkable reversal in sign of the phase velocity around 80 km that is not found at our location. In general we interpret the differences in amplitudes (decreasing with decreasing latitude) and phases as latitudinal differences in temperature structure due to the residual pole-to-pole circulation.

For the stratopause region annual and semi-annual components have been derived from SAGE II satellite based observations for different latitude bands (Burton and Thomason, 2003). The most suitable latitude band is centered around 60° N. Here the annual amplitude is about twice as large as our results, while the semi-annual component is only half. This difference can be explained by the large integration range of the SAGE II analysis, covering about 20° in latitude. Phases are again similar to our observations.

Comparison with other latitudes reveals the position of our site at the edge between polar and mid-latitudes. Above we have compared our results mainly with observations between 40° N and 44° N, where several lidars exist. Towards the north the observational sites get sparse. Nevertheless a comparison is made for different specific features of the middle atmosphere.

The summer mesopause temperature is decreasing from mid-latitudes towards the north pole. At ∼40° N the summer mesopause temperature is about 167 K as recently published from full-diurnal data by Yuan et al. (2008) for the period May 2002 to April 2006, i.e. comparable to our sounding period. Our data reveal nighttime temperatures of ∼144 K while Lübken (1999) report 129 K for 69° N. Recent observations of Höffner and Lübken (2007) show summer mesopause temperatures as low as ∼120 K at 78° N.

The same studies show that differences between summer and winter mesopause temperatures increase with latitude. The differences are about 10 K, 25 K and 60 K at ∼40° N, 54° N and 78° N, respectively. The increasing differences are mostly due to decreasing summer mesopause temperatures, while the winter mesopause temperatures are more constant at ∼175–190 K. The summer mesopause temperatures are due to a wave driven upwelling that is much stronger in polar regions compared to lower latitudes. As mentioned before, the Kühlungsborn latitude of 54° N is at the edge of the polar region, with the slope of summer mesopause temperatures being steeper towards lower latitudes (∼1.7 K/deg) than towards higher latitudes (∼1.2 K/deg).

Also the date of lowest temperatures show some remarkable variation with latitude. While the lowest temperatures at ∼40° N and also at 54° N (this site) are reached around or shortly before summer solstice (cf. fit results given by Leblanc et al. (1998); States and Gardner (2000)), they appear at polar latitudes with a shift of 1–2 weeks compared to summer solstice (Lübken, 1999; Höffner and Lübken, 2007). It remains an open question why the minimal temperatures are reached earlier in time in mid-latitudes, as the upwelling from the best of out knowledge starts in polar regions.

Stratopause temperatures show only small variations with latitude. Summarizing the observations at 41/44° N, Leblanc et al. (1998) presented a summer stratopause temperature of 280–290 K. This is about 10 K higher than the observations at 54° N (this data) and at 69° N Schöch et al. (2008). At all latitudes winter stratopause temperatures are influenced by stratospheric disturbances, resulting in only slightly lower temperatures compared to the particular summer data.

8 Conclusions and summary

We have described the temperature structure of the Earth's atmosphere at 54° N and its seasonal variation in the whole altitude range between 1 and 105 km (troposphere to lower thermosphere). The study is based on about six years of observations, i.e. 266 nights of 3–15 h sounding time (totally nearly 1900 h). We have compiled a unique

data set of uninterrupted profiles that are observed by the same technique (lidar). For the first time temperature profiles have been combined from Raman-, Rayleigh-, and resonant backscatter lidars at the same location, providing comparable spatiotemporal resolution over the whole altitude range.

Seasonal temperature variations at mid-latitudes have already been published before (e.g. She and von Zahn, 1998; Leblanc et al., 1998). In our study we have extended the existing data set strongly and have concentrated on the latitude of 54° N. This latitude range is of particular importance as it connects polar phenomena like Sudden Stratospheric Warmings (SSW) and Noctilucent Clouds (NLC) with mid-latitudes. In summer the mesopause temperature is as low as ∼144 K, i.e. the existence of ice particles is possible for a couple of weeks and in a small altitude range between about 85 and 90 km. In winter temperature profiles are also affected by Stratospheric Warmings and Mesospheric Coolings. Due to this transient phenomena the standard deviation of the nightly mean profiles in January is as large as 20 K at 40 km altitude and the winter stratopause temperature is about as high as in summer.

Regarding the vertical temperature structure our study generally confirms the findings of Leblanc et al. (1998) who combined observations from different stations to get a temperature field between the stratosphere and the lower thermosphere. Nevertheless there are distinct differences due to our more "polar" location. We have used harmonic fits of the temperature field at any altitude bin to reduce effects of natural variability and incomplete sampling of the seasonal temperature distribution. Overall, the harmonic fit of annual, semi-annual and quarter-annual variation nicely reproduces the observed temperature structure. Typically, the differences between observed and fitted temperatures are less than 5 K and are due to the above mentioned natural inter-annual and day-to-day variability. The influence of SSW on the temperature profiles is reduced, but the result of the harmonic analysis still shows a semi-annual variation in stratopause altitudes. The semi-annual amplitude is about as large as the annual variation with maximum in summer.

Comparing amplitudes of the different harmonics, the annual variation is always

dominating and nearly ±27 K in the mesopause region. The quarter-annual variation is smallest, with amplitudes of less than 3 K. In the MLT (mesosphere/lower thermosphere) region (~70–100 km) the amplitude of the annual and semi-annual variations are larger than observed at mid-latitude stations around 40°N (Leblanc et al., 1998), but much lower than e.g. observed near 90 km at polar latitudes of 78° N (Höffner and Lübken, 2007). The annual variation is driven by the residual pole-to-pole circulation, which has largest effects in the polar regions. Accordingly, the slope of mesopause temperatures with latitude is larger equatorward of our site compared to the poleward direction. This again demonstrates the importance of our observations at the edge of the polar region.

From the harmonic analysis we yield a downward propagation of temperature changes, with a phase velocity of about −0.4 km/d between 45 and 90 km altitude (semi-annual) or between 70 and 90 km altitude (annual). This reveals the general importance of waves for the seasonal temperature variation. Additionally, the phase jump of the annual component around 65 km describes the transition between the radiatively driven stratosphere (warm summer) and the dynamically driven MLT (cold summer).

The temperature variation at stratopause heights is roughly symmetric to the solstices. The stratopause temperature has a semi-annual cycle with maxima in winter and summer (266 K and 276 K, respectively) and minima in spring and autumn (263 K and 257 K, respectively). The average stratopause altitude is nearly constant throughout the year, varying only between 47 and 49 km. The mesopause has been identified at temperatures as low as 144 K in summer and about 170 K in winter. The mesopause altitude varies between ~102 km in winter and 86/87 km in summer, with a transition phase of about two weeks or less. This sharp transition allows to identify a "summer season" (indicated by a low mesopause) with a length of about 120 days. The temperature minimum of the summer mesopause is observed around day 169, i.e. nearly at summer solstice. This is comparable to measurements near 40° N, but in contrast to the observation of a 1–2 week phase shift at higher latitudes.

Our data set reveals some discrepancies compared to the most recent NRLMSISE-

00 reference atmosphere and satellite observations. The MSIS temperatures are generally too high in the whole range between 70 and 105 km and for nearly all seasons. The available satellite observations show the largest discrepancies in the summer mesopause region. Here they provide typically too low temperatures and a too low mesopause, which are e.g. not in agreement with local observations of Noctilucent Clouds. The largest drawback of our own temperature profiles is the limited daily coverage. Actually we aim for complete daylight capabilities for the range 30–105 km to avoid potential influences of solar tides on the mean temperatures.

Acknowledgements. We acknowledge the support in lidar operation and maintenance of T. Köpnick and M. Priester. Additionally, we would like to thank numerous students for their help in nighttime lidar soundings. Parts of this work were supported by the Deutsche Forschungsgemeinschaft (DFG) under grant GE 1625/1-1.

References

Alpers, M., Eixmann, R., Fricke-Begemann, C., Gerding, M., and Höffner, J.: Temperature lidar measurements from 1 to 105 km altitude using resonance, Rayleigh, and rotational Raman scattering, Atmos. Chem. Phys., 4, 793–800, 2004, http://www.atmos-chem-phys.net/4/793/2004/. 16179, 16181

Andrews, D. G., Holton, J. R., and Leovy, C. B.: Middle atmosphere dynamics, vol. 40 of International Geophysics Series, Academic Press, Orlando, USA, 1 edn., 1987. 16177

Berger, U. and von Zahn, U.: The two-level structure of the mesopause: a model study, J. Geophys. Res., 104, 22 083–22 093, 1999. 16183

Burton, S. P. and Thomason, L. W.: Molecular density retrieval and temperature climatology for 40–60 km from SAGE II, J. Geophys. Res., 108, 4593, doi:10.1029/2003JD003605, 2003. 16196

Chen, S., Hu, Z., White, M. A., Chen, H., Krueger, D. A., and She, C.-Y.: Lidar observations of seasonal variation of diurnal mean temperature in the mesopause region over Fort Collins, Colorado (41° N, 105° W), J. Geophys. Res., 105, 12 371–12 379, 2000. 16195

Eska, V., Höffner, J., and von Zahn, U.: Upper atmosphere potassium layer and its seasonal variations at 54° N, J. Geophys. Res., 103, 29 207–29 214, 1998. 16180, 16182

Faduilhe, D., Keckhut, P., Bencherif, H., Roberta, L., and Baldy, S.: Stratospheric temperature monitoring using a vibrational Raman lidar – Part 1: Aerosols and ozone interferences, J. Environ. Monit., 7, 357–364, 2005. 16192

Fricke-Begemann, C. and Höffner, J.: Temperature tides and waves near the mesopause from lidar observations at two latitudes, J. Geophys. Res., 110, D19103, doi:10.1029/2005JD005770, 2005. 16193

Friedman, J. S. and Chu, X.: Nocturnal temperature structure in the mesopause region over the Arecibo observatory (18.35° N, 66.75° W): Seasonal variations, J. Geophys. Res., 112, D14107, doi:10.1029/2006JD008220, 2007. 16178

Fromm, M., Alfred, J., and Pitts, M.: A unified, long-term, high-latitude stratospheric aerosol and cloud data base using SAM II, SAGE II, and POAM II/III data: Algorithm description, data base definition, and climatology, J. Geophys. Res., 108, 1–17, 2003. 16193

Garcia, R. R.: Dynamics, radiation and photochemistry in the mesosphere: Implications for the formation of noctilucent clouds, J. Geophys. Res., 94, 14 605–14 615, 1989. 16176

Gerding, M., Höffner, J., Rauthe, M., and Lübken, F.-J.: Observations of noctilucent clouds and temperature structure from 1–105 km by co-located lidars at 54° N, in: Proceedings of the SPIE symposium "Lidar Technologies, Techniques, and Measurements for Atmospheric Remote Sensing II", edited by: Singh, U., SPIE Proceedings, Bellingham, WA, USA, 636705, doi:10.1117/12.689012, 2006. 16181

Gerding, M., Höffner, J., and Rauthe, M.: Simultaneous observations of temperatures and ice-particles in the mid-latitude mesopause region, Adv. Space Res., 40, 785–793, 2007a. 16195

Gerding, M., Höffner, J., Rauthe, M., Singer, W., Zecha, M., and Lübken, F.-J.: Simultaneous observation of NLC, MSE and temperature at a mid-latitude station (54° N), J. Geophys. Res., 112, D12111, doi:10.1029/2006JD008135, 2007b. 16178, 16192, 16195

Gobiet, A., Foelsche, U., Steiner, A. K., Borsche, M., Kirchengast, G., and Wickert, J.: Climatological validation of stratospheric temperatures in ECMWF operational analyses with CHAMP radio occultation data, Geophys. Res. Lett., 32, L12806, doi:10.1029/2005GL022617, 2005. 16178

Gross, M. R., McGee, T. J., Ferrare, R. A., Singh, U. N., and Kimvilakani, P.: Temperature measurements made with a combined Rayleigh-Mie and Raman lidar, Appl. Opt., 36, 5987–5995, 1997. 16192

Hagan, M. E. and Forbes, J. M.: Migrating and nonmigrating diurnal tides in the middle and

upper atmosphere excited by tropospheric latent heat release, J. Geophys. Res., 107, 4754, doi:10.1029/2001JD001236, 2002. 16193
Hauchecorne, A., Chanin, M. L., and Keckhut, P.: Climatology and trends of the middle atmospheric temperature (33–87 km) as seen by Rayleigh lidar over the south of France, J. Geophys. Res., 96, 15 297–15 309, 1991. 16178
Hirota, I.: Climatology of gravity waves in the middle atmosphere, J. Atmos. Terr. Phys., 46, 767–773, 1984. 16178
Höffner, J. and Lübken, F.-J.: Potassium lidar temperatures and densities in the mesopause region at Spitsbergen (78° N), J. Geophys. Res., 112, D20114, doi:10.1029/2007JD008612, 2007. 16196, 16197, 16199
Holton, J. R.: The role of gravity wave induced drag and diffusion in the momentum budget of the mesosphere, J. Atmos. Sci., 39, 791–799, 1982. 16177
Huang, F. T., Mayr, H. G., Reber, C. A., Killeen, T., Russell, J., Mlynczak, M., Skinner, W., and Mengel, J.: Diurnal variations of temperature and winds inferred from TIMED and UARS measurements, J. Geophys. Res., 111, A10S04, doi:10.1029/2005JA011426, 2006. 16193
Huang, F. T., Mayr, H. G., Reber, C. A., Russell, J. M., Mlynczak, M., and Mengel, J. G.: Stratospheric and mesospheric temperature variations for the quasi-biennial and semiannual (QBO and SAO) oscillations based on measurements from SABER (TIMED) and MLS (UARS), Ann. Geophys., 12, 2131–2149, 2006, http://www.ann-geophys.net/12/2131/2006/. 16195, 16196
Kubicki, A., Keckhut, P., Chanin, M.-L., Hauchecorne, A., Lysenko, E., and Golitsyn, G. S.: Temperature trends in the middle atmosphere as seen by historical Russian rocket launches – Part 1: Volgograd (48.68° N, 44.35° E), J. Atmos. Solar-Terr. Phys., 68, 1075–1086, 2006. 16178
Kutepov, A. A., Feofilov, A. G., Marshall, B. T., Gordley, L. L., Pesnell, W. D., Goldberg, R. A., and Russell III, J. M.: SABER temperature observations in the summer polar mesosphere and lower thermosphere: importance of accounting for the CO_2 v_2 quanta V–V exchange, Geophys. Res. Lett., 33, L21809, doi:10.1029/2006GL026591, 2006. 16177, 16191, 16195
Leblanc, T., McDermid, I. S., Keckhut, P., Hauchecorne, A., She, C.-Y., and Krueger, D. A.: Temperature climatology of the middle atmosphere from long-term lidar measurements at middle and low latitudes, J. Geophys. Res., 103, 17 191–17 204, 1998. 16178, 16195, 16196, 16197, 16198, 16199
Lindzen, R. S.: Turbulence and stress owing to gravity wave and tidal breakdown, J. Geophys.

Res., 86, 9707–9714, 1981. 16177
Lübken, F.-J.: Thermal structure of the Arctic summer mesosphere, J. Geophys. Res., 104, 9135–9149, 1999. 16178, 16196, 16197
Lübken, F.-J., Zecha, M., Höffner, J., and Röttger, J.: Temperatures, polar mesosphere summer echoes, and noctilucent clouds over Spitsbergen (78° N), J. Geophys. Res., 109, D11203, doi:10.1029/2003JD004247, 2004. 16178
Meriwether, J. W. and Gerrard, A. J.: Mesosphere inversion layers and stratosphere temperature enhancements, Rev. Geophys., 42, RG3003, doi:10.1029/2003RG000133, 2004. 16184
Mertens, C. J.: Retrieval of mesospheric and lower thermospheric kinetic temperature from measurements of CO_2 15 μm earth limb emission under non-LTE conditions, Geophys. Res. Lett., 28, 1391–1394, 2001. 16177
Mlynczak, M. G. and Solomon, S.: A detailed evaluation of the heating efficiency in the middle atmosphere, J. Geophys. Res., 98, 10 517–10 541, 1993. 16177
Picone, J. M., Hedin, A. E., Drob, D. P., and Aikin, A. C.: NRLMSISE-00 empirical model of the atmosphere: statistical comparison and scientific issues, J. Geophys. Res., 107, 1468, doi:10.1029/2002JA009430, 2002. 16179, 16190
Rauthe, M., Gerding, M., Höffner, J., and Lübken, F.-J.: Lidar temperature measurements of gravity waves over Kühlungsborn (54° N) from 1 to 105 km: a winter-summer comparison, J. Geophys. Res., 111, D24108, doi:10.1029/2006JD007354, 2006. 16184
Rauthe, M., Gerding, M., and Lübken, F.-J.: Seasonal changes in gravity wave activity measured by lidars at mid-latitudes, Atmos. Chem. Phys. Discuss., 8, 13 741–13 773, 2008, http://www.atmos-chem-phys-discuss.net/8/13741/2008/. 16178, 16183, 16184
Riese, M., Offermann, D., and Brasseur, G.: Energy released by recombination of atomic oxygen and related species at mesopause heights, J. Geophys. Res., 99, 14 585–14 593, 1994. 16177
Schöch, A., Baumgarten, G., and Fiedler, J.: Polar middle atmosphere temperature climatology from Rayleigh lidar measurements at ALOMAR (69° N), Ann. Geophys., 26, 1681–1698, 2008, http://www.ann-geophys.net/26/1681/2008/. 16197
She, C. Y. and von Zahn, U.: Concept of a two-level mesopause: Support through new lidar observations, J. Geophys. Res., 103, 5855–5863, 1998. 16192, 16194, 16198
She, C.-Y., Yu, J. R., and Chen, H.: Observed thermal structure of a midlatitude mesopause, Geophys. Res. Lett., 20, 567–570, 1993. 16183

Shepherd, M. G., Reid, B., Zhang, S., Solheim, B. H., and Shepherd, G. G.: Retrieval and validation of mesospheric temperatures from Wind Imaging Interferometer observations, J. Geophys. Res., 106, 24 813–24 829, 2001. 16177

Sica, R. J., Izawa, M. R. M., Walker, K. A., Boone, C., Petelina, S. V., Argall, P. S., Bernath, P., Burns, G. B., Catoire, V., Collins, R. L., Daffer, W. H., De Clercq, C., Fan, Z. Y., Firanski, B. J., French, W. J. R., Gerard, P., Gerding, M., Granville, J., Innis, J. L., Keckhut, P., Kerzenmacher, T., Klekociuk, A. R., Kyr, E., Lambert, J. C., Llewellyn, E. J., Manney, G. L., McDermid, I. S., Mizutani, K., Murayama, Y., Piccolo, C., Raspollini, P., Ridolfi, M., Robert, C., Steinbrecht, W., Strawbridge, K. B., Strong, K., Stbi, R., and Thurairajah, B.: Validation of the Atmospheric Chemistry Experiment (ACE) version 2.2 temperature using ground-based and space-borne measurements, Atmos. Chem. Phys., 8, 35–62, 2008, http://www.atmos-chem-phys.net/8/35/2008/. 16177, 16191

States, R. J. and Gardner, C. S.: Thermal structure of the mesopause region (80 – 105 km) at 40° N latitude – Part 1: Seasonal variations, J. Atmos. Sci., 57, 66–77, 2000. 16178, 16192, 16193, 16197

Vaughan, G. and Wareing, D. P.: Stratospheric aerosol measurements by dual polarisation lidar, Atmos. Chem. Phys., 4, 2441–2447, 2004, http://www.atmos-chem-phys.net/4/2441/2004/. 16181, 16194

von Zahn, U. and Höffner, J.: Mesopause temperature profiling by potassium lidar, Geophys. Res. Lett., 23, 141–144, 1996. 16179

Wickwar, V. B., Beissner, K. C., Wilkerson, T. D., Collins, S. C., Maloney, J. M., Meriwether Jr., J. W., and Gao, X.: Climatology of mesospheric temperature profiles observed with the Consortium Rayleigh-scatter lidar at Logan, Utah, in: Advances in Atmospheric Remote Sensing with Lidar, edited by: Ansmann, A., Neuber, R., Rairoux, P., and Wandinger, U., Springer-Verlag, Berlin, Germany, 557–560, 1997. 16178

Xu, J., Liu, H.-L., Yuan, W., Smith, A. K., Roble, R. G., Mertens, C. J., Russell III, J. M., and Mlynczak, M. G.: Mesopause structure from Thermosphere, Ionosphere, Mesosphere, Energetics, and Dynamics (TIMED)/Sounding of the Atmosphere using Broadband Emission Radiometry (SABER) observations, J. Geophys. Res., 112, D09102, doi:10.1029/2006JD007711, 2007. 16177, 16194, 16195

Yu, J. R. and She, C.-Y.: Climatology of a midlatitude mesopause region observed by a lidar at Fort Collins, Colorado (40.6° N, 105° W), J. Geophys. Res., 100, 7441–7452, 1995.

Yuan, T., She, C.-Y., Krueger, D. A., Sassi, F., Garcia, R., Roble, R. G., Liu, H.-L., and Schmidt, H.: Climatology of mesopause region temperature, zonal wind, and meridional wind over Fort Collins, Colorado (41° N, 105° W), and comparison with model simulations, J. Geophys. Res., 113, D03105, doi:10.1029/2007JD008697, 2008. 16178

16193, 16196

Table 1. Monthly mean temperatures [K] between 2 and 104 km from all soundings longer than 3 h.

altitude [km]	Jan	Feb	Mar	Apr	May	Jun	Jul	Aug	Sep	Oct	Nov	Dec
104	167.2	162.2	165.1	166.7	–	–	–	178.4	174.5	176.4	–	–
102	172.0	167.5	164.5	169.1	171.6	183.6	178.4	170.8	168.7	175.3	–	–
100	178.4	170.3	168.7	166.5	166.6	176.5	176.1	178.1	172.7	178.6	178.2	165.8
98	183.4	174.3	170.9	167.7	165.1	173.4	169.5	176.0	176.6	180.5	177.4	168.4
96	186.9	176.1	175.5	166.9	162.6	168.9	168.3	173.4	178.3	182.7	182.1	171.4
94	190.3	178.9	179.3	168.7	161.2	163.8	164.2	172.4	181.0	185.4	185.5	174.0
92	194.8	182.1	182.4	171.1	160.4	157.9	160.7	171.4	185.0	187.6	190.6	177.8
90	198.2	185.6	184.4	173.9	158.8	152.0	156.2	171.1	188.2	190.6	196.8	181.7
88	202.5	187.5	185.4	175.9	155.3	147.1	150.9	167.8	188.6	193.2	200.7	186.3
86	206.0	190.9	188.4	178.8	154.5	145.8	147.6	163.4	187.4	195.5	203.9	190.7
84	208.2	196.6	193.9	183.7	161.9	152.5	155.3	165.9	188.0	197.4	209.0	198.0
82	210.8	202.9	196.9	188.8	171.0	160.6	162.7	173.4	193.3	202.1	213.7	204.9
80	212.7	208.9	201.3	195.3	178.6	168.9	169.7	179.5	193.9	203.9	219.7	209.5
78	213.5	213.5	204.6	199.4	186.0	177.0	176.3	183.6	195.1	204.7	221.5	211.9
76	216.0	216.8	208.9	204.0	193.7	185.1	183.4	188.3	197.1	206.7	222.6	214.1
74	218.9	219.8	214.2	208.3	201.5	193.5	190.8	194.2	199.2	211.6	224.9	216.9
72	221.0	223.2	219.2	212.7	209.6	202.6	199.3	200.5	202.7	217.6	227.0	218.8
70	221.9	227.6	224.1	217.9	216.4	211.8	208.2	207.2	207.4	223.3	228.9	219.5
68	222.6	230.3	229.1	223.9	223.7	220.8	217.5	214.9	212.6	227.9	230.0	221.6
66	224.8	232.5	233.9	229.9	231.2	229.9	226.9	222.7	218.8	231.3	233.1	225.6
64	228.4	236.6	238.6	236.0	238.4	238.5	234.9	230.5	225.7	234.0	236.5	230.1
62	231.5	241.0	242.2	241.7	245.1	246.2	242.7	238.0	232.2	237.4	241.2	234.1
60	236.9	245.0	246.0	247.0	250.8	253.0	249.5	245.5	239.1	240.2	245.2	240.5
58	242.4	248.5	249.4	252.4	256.1	258.6	256.1	251.8	245.2	244.4	248.2	246.8
56	246.8	251.7	252.9	256.7	261.4	264.0	261.3	257.2	251.1	248.0	250.7	251.1
54	251.4	254.5	256.2	261.3	265.3	268.2	265.1	261.9	255.8	251.1	252.8	258.5

ACPD
8, 16175–16218, 2008

Table 1. Continued.

altitude [km]	Jan	Feb	Mar	Apr	May	Jun	Jul	Aug	Sep	Oct	Nov	Dec
52	254.1	258.2	258.9	264.6	268.2	270.9	268.4	265.4	259.2	253.6	254.0	267.5
50	258.3	260.9	260.7	266.8	270.0	272.2	270.5	267.4	261.6	255.2	253.8	274.5
48	263.3	261.2	261.1	268.1	271.0	273.0	271.3	268.0	262.4	256.0	252.8	279.0
46	265.6	259.4	260.2	267.1	271.4	272.3	270.9	266.9	261.5	254.9	250.0	277.0
44	267.1	257.3	258.1	265.1	269.2	270.7	268.2	264.7	259.3	252.7	246.1	272.8
42	267.2	253.5	253.5	261.1	264.8	267.1	263.6	260.8	255.4	248.5	240.4	262.7
40	263.7	246.4	248.3	255.2	259.1	261.3	258.8	255.9	250.5	243.1	233.7	250.6
38	256.4	238.6	243.1	248.9	253.5	255.1	253.6	250.5	245.3	237.6	226.2	239.2
36	246.6	230.8	237.7	242.4	247.2	249.4	248.1	245.2	239.7	232.1	219.7	227.8
34	235.4	222.9	232.2	235.9	240.5	243.3	242.8	239.6	234.3	226.9	214.0	216.8
32	223.4	215.5	227.2	230.0	233.9	237.5	237.7	235.4	230.1	221.4	208.7	208.4
30	213.8	212.3	223.4	225.1	229.2	233.7	233.8	231.4	226.4	218.7	206.7	204.7
28	207.8	210.6	220.3	221.7	225.2	230.0	230.6	228.6	223.5	216.5	207.3	202.5
26	205.4	209.7	217.3	219.9	222.4	226.7	227.5	226.4	221.2	215.2	210.0	202.5
24	204.4	210.6	216.0	219.2	221.1	224.6	225.1	224.1	219.8	214.6	211.8	205.1
22	205.3	211.7	215.9	219.3	220.9	223.5	225.1	222.7	219.1	214.1	213.3	207.4
20	206.0	214.0	215.4	219.5	221.4	223.7	224.9	222.9	218.8	214.9	214.2	210.7
18	207.8	213.8	215.2	219.1	221.1	222.9	224.3	221.6	217.6	214.9	215.0	211.8
16	209.9	215.0	215.4	219.4	221.1	222.5	224.3	220.9	216.1	214.7	215.6	213.9
14	211.8	215.9	214.7	218.9	221.7	222.0	224.0	220.9	215.3	215.4	215.8	213.9
12	211.3	214.5	212.8	216.6	220.0	221.8	223.6	221.8	217.9	216.5	216.2	212.7
10	214.5	216.2	217.0	219.7	223.0	228.5	231.7	229.7	228.3	222.1	221.7	219.1
8	226.7	226.0	230.8	234.2	237.0	243.7	247.7	244.6	243.8	235.3	232.3	234.5
6	242.5	239.3	246.9	250.6	252.5	259.5	263.0	259.3	259.3	249.9	246.5	250.7
4	257.7	252.5	260.7	265.0	266.3	271.9	274.8	271.2	271.6	262.6	259.9	264.4
2	264.0	268.1	265.0	273.3	275.3	283.3	281.5	286.4	285.1	272.6	275.4	281.8

Table 2. Parameters of the harmonic fit with annual, semi-annual and quarter-annual variation. The phase describes the day with maximum temperatures.

altitude [km]	annual mean	Amplitude [km] annual	1/2-annual	1/4-annual	Phase [d] annual	1/2-annual	1/4-annual
104	173.8	8.1	5.7	1.0	220.5	167.2	74.6
102	172.2	3.0	4.0	1.5	242.0	164.5	25.8
100	173.4	4.3	2.5	1.2	279.2	12.2	26.2
98	174.2	5.8	1.7	0.4	317.6	36.4	41.3
96	175.0	8.8	2.3	0.2	333.3	50.5	79.5
94	175.9	11.9	3.9	0.4	342.3	67.6	74.1
92	177.1	15.5	6.1	0.5	346.6	74.1	66.7
90	178.2	19.3	8.2	0.5	348.7	78.2	49.6
88	178.5	23.7	9.1	0.4	351.3	80.9	8.9
86	179.5	27.1	9.3	1.7	355.7	84.8	0.9
84	184.2	26.4	7.4	2.3	359.4	86.4	3.4
82	190.0	24.6	6.5	1.8	358.6	89.0	6.5
80	195.0	22.5	5.0	1.2	362.9	94.0	16.0
78	198.7	19.8	3.9	0.8	1.4	98.7	26.0
76	202.8	17.2	3.0	0.6	6.5	103.9	32.1
74	207.7	15.2	2.6	0.9	9.8	116.7	35.3
72	212.9	12.5	2.8	1.0	12.7	128.7	37.1
70	218.1	9.4	2.9	1.1	17.9	132.6	36.2
68	223.2	5.9	3.0	1.5	32.1	133.8	34.9
66	228.6	3.6	3.0	1.4	65.0	140.0	38.6
64	234.2	3.7	2.8	1.4	107.9	146.5	44.5
62	239.6	4.8	2.8	1.6	136.5	151.5	48.4
60	244.9	5.8	2.7	1.6	148.7	160.0	52.1
58	250.0	6.4	2.7	1.2	156.0	165.4	53.5
56	254.4	7.3	2.7	1.2	161.8	167.4	56.3
54	258.4	7.4	2.9	1.1	162.8	169.4	59.3

ACPD
8, 16175–16218, 2008

Table 2. Continued.

altitude [km]	annual mean	Amplitude [km] annual	1/2-annual	1/4-annual	Phase [d] annual	1/2-annual	1/4-annual
52	261.7	6.9	3.2	1.2	162.3	173.1	64.9
50	264.1	6.1	3.6	1.1	159.0	176.9	70.3
48	265.4	5.2	4.5	1.2	152.8	178.4	80.1
46	264.6	5.3	4.9	1.4	149.9	179.9	86.5
44	262.6	5.2	5.3	1.9	144.0	181.9	90.2
42	258.4	5.5	5.4	2.0	141.6	2.5	2.1
40	252.5	6.2	5.0	2.2	147.7	7.0	5.8
38	246.0	7.4	4.1	2.2	155.4	12.1	8.1
36	239.2	9.1	3.3	2.0	162.5	18.9	8.7
34	232.3	10.8	2.5	1.9	168.6	30.1	8.9
32	225.9	12.7	2.4	1.3	174.2	48.7	7.3
30	221.7	13.1	2.1	0.8	178.1	58.7	0.6
28	218.7	12.8	2.2	0.5	180.8	64.9	89.7
26	216.9	11.5	1.8	0.2	183.4	70.9	88.6
24	216.2	10.0	1.5	0.2	183.6	79.5	67.7
22	216.2	8.9	1.2	0.1	182.0	78.3	65.6
20	216.9	8.0	0.7	0.0	181.9	82.9	3.5
18	216.8	6.9	0.1	0.3	181.0	134.5	23.0
16	217.1	5.8	0.6	0.7	174.8	165.6	22.2
14	217.3	5.1	1.0	1.2	174.1	168.2	23.7
12	217.0	5.3	0.9	0.8	195.4	172.4	25.3
10	222.5	7.7	1.1	0.3	211.5	13.3	75.6
8	236.1	9.7	1.1	1.1	207.4	19.4	86.0
6	251.3	10.0	0.8	1.8	203.9	13.6	87.2
4	264.5	8.8	0.7	2.0	200.9	176.2	87.6
2	276.0	9.0	2.1	1.5	216.8	0.1	66.1

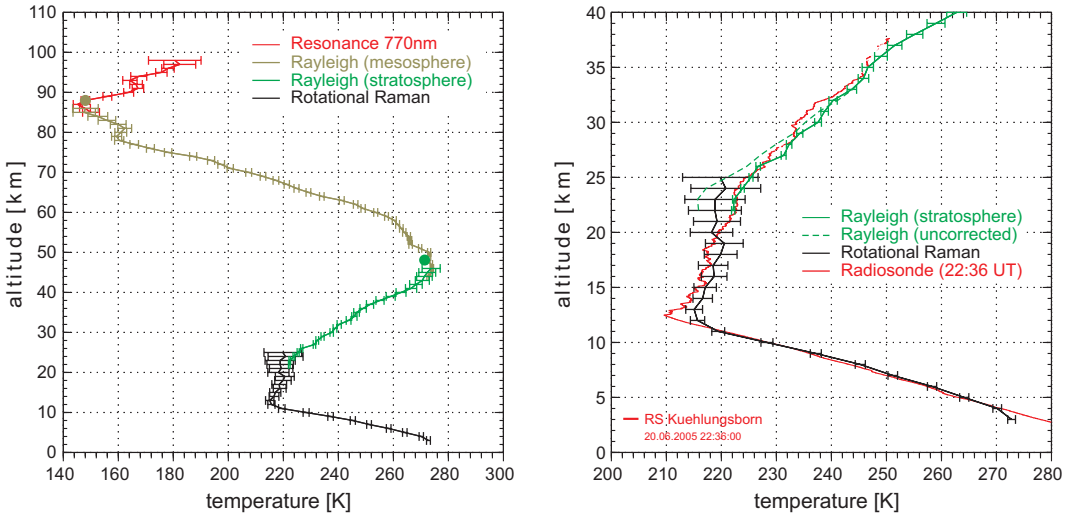

Fig. 1. Temperature profile from combined soundings after one hour of integration (20 June 2005, 22:30–23:30 UT). Left: complete altitude range, right: detailed view on troposphere/lower stratosphere with comparison to co-located radiosonde.

ACPD
8, 16175–16218, 2008

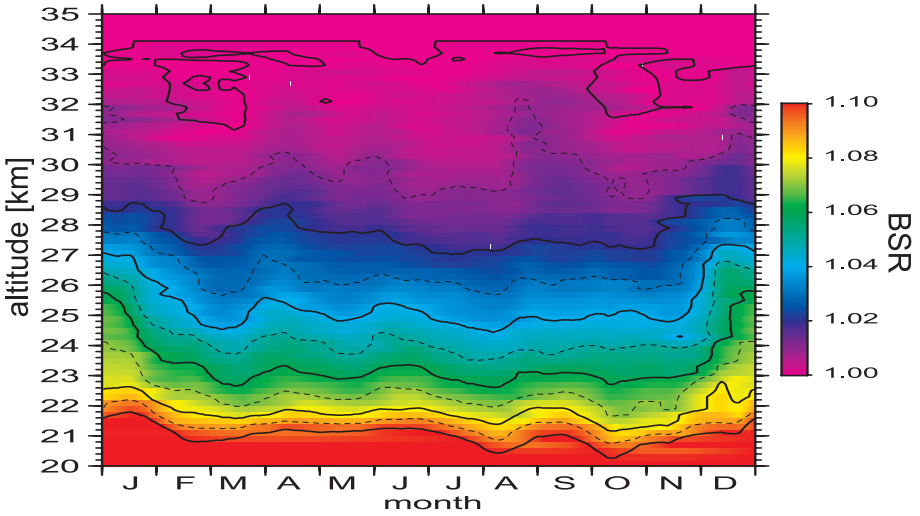

Fig. 2. Seasonal variation of backscatter ratios (BSR) at 532 nm wavelength (213 nights, 11 February 2004–31 July 2007).

ACPD
8, 16175–16218, 2008

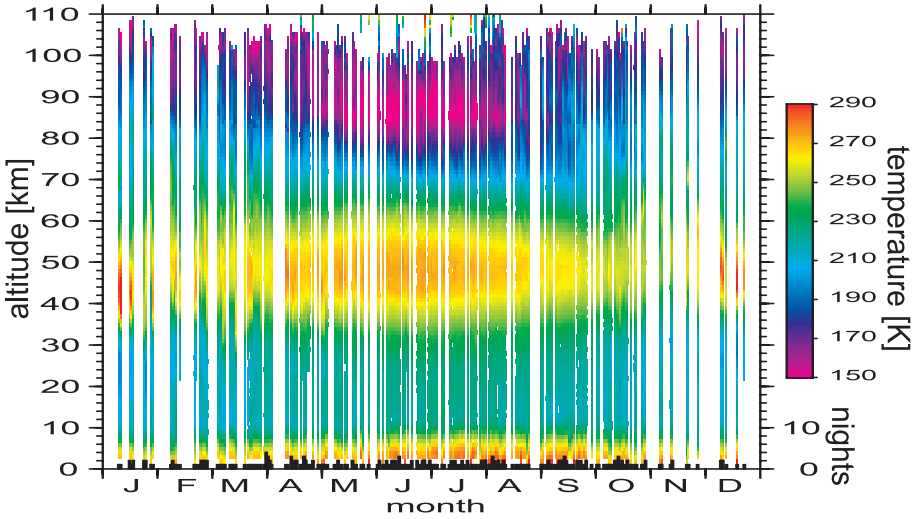

Fig. 3. Seasonal variation of nightly mean temperatures between 1 and ~110 km altitude. The black histogram denotes the number of soundings with the particular date (right axis).

ACPD
8, 16175–16218, 2008

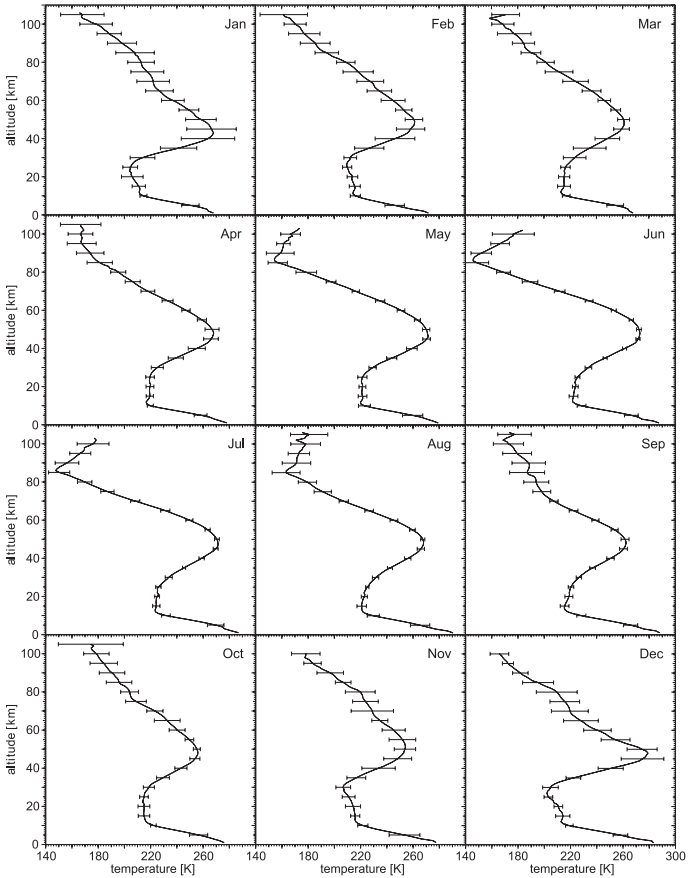

Fig. 4. Monthly averages of nightly mean temperatures between 1 and ~110 km altitude. The horizontal bars denote the standard deviations of the nightly mean temperatures (i.e. natural variability but not statistical uncertainties).

ACPD
8, 16175–16218, 2008

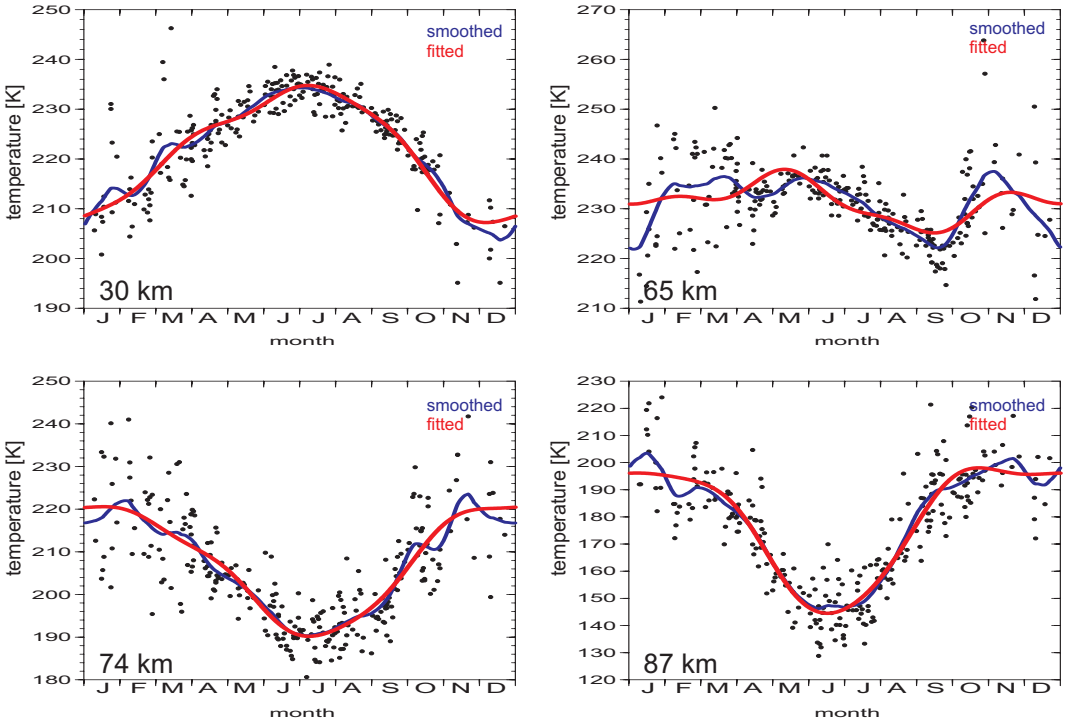

Fig. 5. Seasonal temperature variation at different altitudes. Black dots: nightly mean temperatures, blue line: filtered with ±30 day Hanning window, red line: harmonic fit.

ACPD
8, 16175–16218, 2008

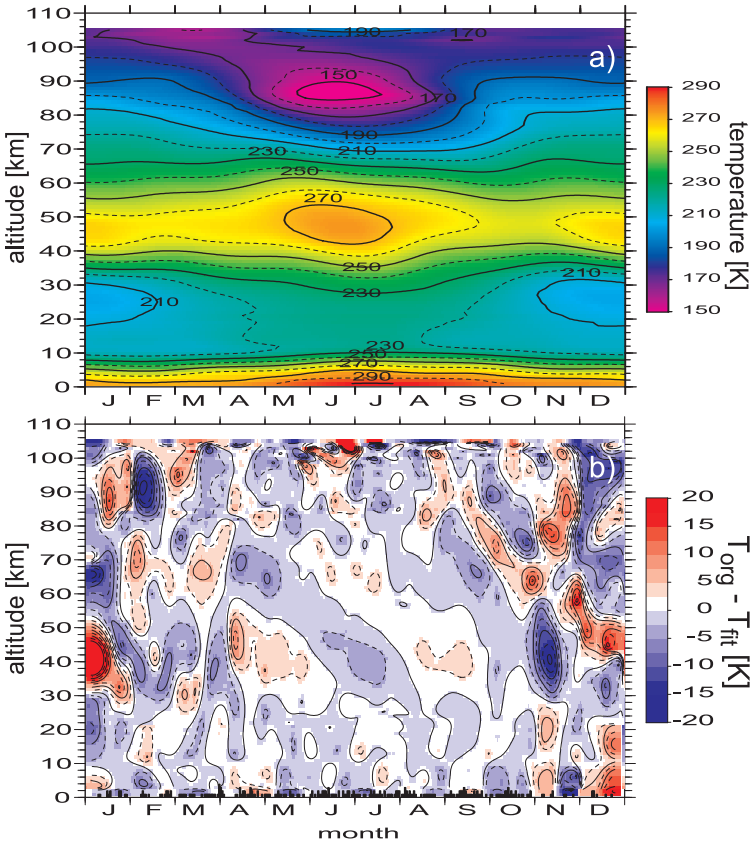

Fig. 6. Temperature structure between 1 and 105 km altitude from harmonic fits with annual, semi-annual and quarter-annual variation **(a)** and difference of the observed structure and the fit results **(b)**.

ACPD
8, 16175–16218, 2008

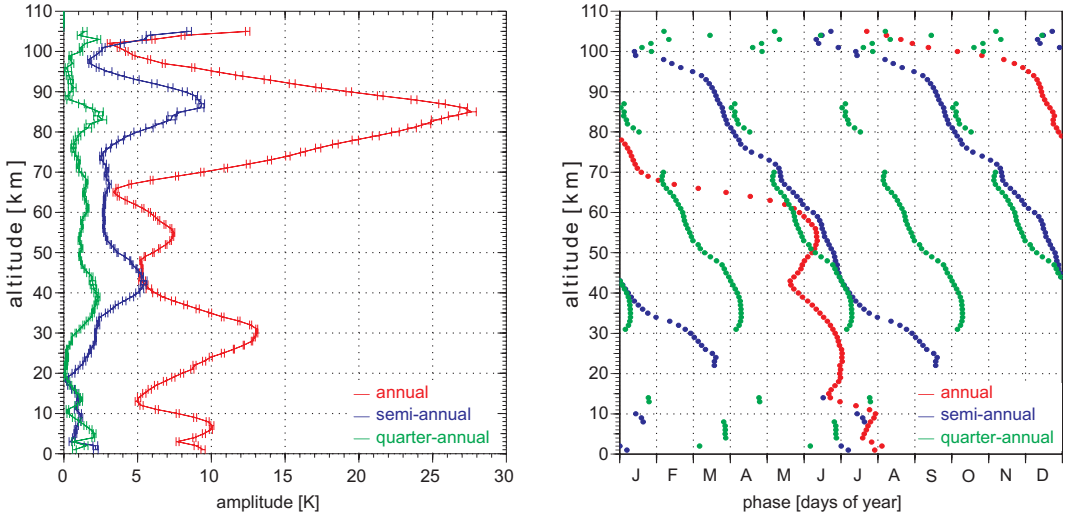

Fig. 7. Amplitudes (left) and phases (right) derived from the harmonic analyses at all altitudes. Phases are only given if the particular amplitude of the cosine-function exceeds 1 K.

ACPD
8, 16175–16218, 2008

Title Page
Abstract Introduction
Conclusions References
Tables Figures
◀◀ ▶▶
◀ ▶
Back Close
Full Screen / Esc
Printer-friendly Version
Interactive Discussion

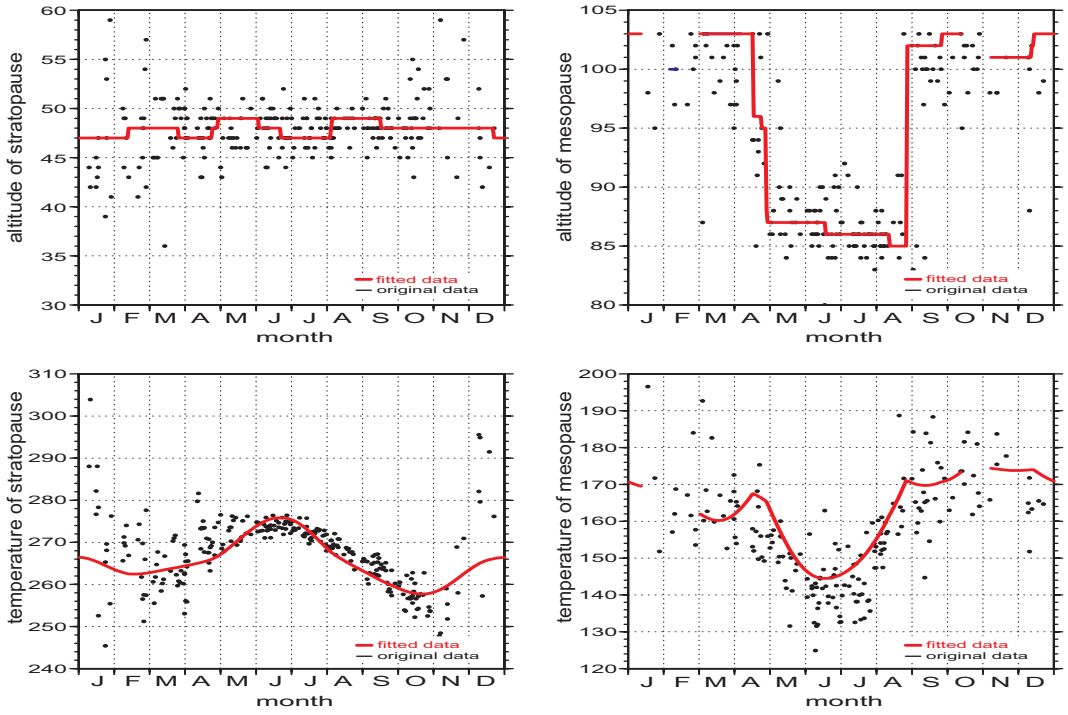

Fig. 8. Altitude (top) and temperature (bottom) of the stratopause (left) and mesopause (right). Dots: results of the nightly mean temperature profiles, red line: results from the fitted temperature structure.

ACPD
8, 16175–16218, 2008

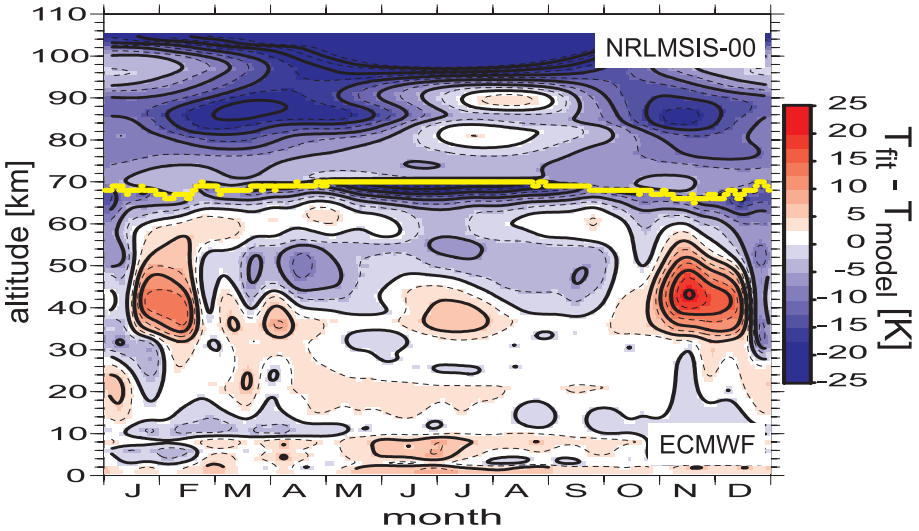

Fig. 9. Difference of fitted lidar observations and reference data sets. Above the yellow line the NRLMSISE-00 is used as reference, below ECMWF-analyses.

ACPD
8, 16175–16218, 2008